




Cite this: *J. Mater. Chem. C*, 2023, **11**, 7750

## Superior high temperature performance of 8 kV NiO/Ga<sub>2</sub>O<sub>3</sub> vertical heterojunction rectifiers

Jian-Sian Li,<sup>a</sup> Chao-Ching Chiang,<sup>a</sup> Xinyi Xia,<sup>a</sup> Hsiao-Hsuan Wan,<sup>a</sup> Fan Ren<sup>a</sup> and S. J. Pearton  \*<sup>ab</sup>

NiO/ $\beta$ -Ga<sub>2</sub>O<sub>3</sub> vertical rectifiers exhibit near-temperature-independent breakdown voltages ( $V_B$ ) of > 8 kV to 600 K. For 100  $\mu$ m diameter devices, the power figure of merit ( $V_B$ )<sup>2</sup>/ $R_{ON}$ , where  $R_{ON}$  is the on-state resistance, was 9.1 GW cm<sup>-2</sup> at 300 K and 3.9 GW cm<sup>-2</sup> at 600 K. By sharp contrast, Schottky rectifiers fabricated on the same wafers show  $V_B$  of  $\sim$ 1100 V at 300 K, with a negative temperature coefficient of breakdown of 2 V K<sup>-1</sup>. The corresponding figures of merit for Schottky rectifiers were 0.22 GW cm<sup>-2</sup> at 300 K and 0.59 MW cm<sup>-2</sup> at 600 K. The on-off ratio remained >10<sup>10</sup> up to 600 K for heterojunction rectifiers but was 3 orders of magnitude lower over the entire temperature range for Schottky rectifiers. The power figure of merit is higher by a factor of approximately 6 than the 1-D unipolar limit of SiC. The reverse recovery times were  $\sim$ 26  $\pm$  2 ns for both types of devices and were independent of temperature. We also fabricated large area, 1 mm<sup>2</sup> rectifiers. These exhibited  $V_B$  of 4 kV at 300 K and 3.6 kV at 600 K. The results show the promise of using this transparent oxide heterojunction for high temperature, high voltage applications.

Received 5th April 2023,  
Accepted 14th May 2023

DOI: 10.1039/d3tc01200j

rsc.li/materials-c

### Introduction

Ultra-wide bandgap semiconductors with bandgaps > 3.4 eV include diamond, AlN and Ga<sub>2</sub>O<sub>3</sub> and have the potential for significantly higher voltage operation with lower switching losses than commercially available SiC and GaN power devices. The various polytypes of Ga<sub>2</sub>O<sub>3</sub> are attracting attention for their potential application in power switching, solar-blind UV detectors and lateral transistors with enhanced two-dimensional electron gas densities.<sup>1–8</sup> It is relatively easy to grow bulk crystals of the stable monoclinic  $\beta$ -polymorph from the melt, which enables large-diameter, high-quality substrates for homoepitaxy at potentially low cost.<sup>2</sup> This is attractive for lower manufacturing costs since the material comprises a significant component of the cost of manufacture.

Ga<sub>2</sub>O<sub>3</sub> has a high critical electric field strength, which allows for higher operating voltages and lower switching losses in power electronics.<sup>1–6</sup> Its ultrawide bandgap also makes it promising for high temperatures and radiation environment applications. As a result of these advantages, Ga<sub>2</sub>O<sub>3</sub> is being considered for several power electronics applications, including inverters, motor drives, and power supplies. There is particular interest in kV-class vertical rectifiers for use in electric vehicles

and their charging infrastructure, as well as power management systems for improved switching efficiency for next generation power grids and efficiently interfacing renewable energy sources with these grids.<sup>1,4,5</sup> One of the goals is to achieve a high breakdown voltage and low on resistance, which is a benefit for rectifiers because of lower switching losses. A figure of merit for power electronic devices is defined as ( $V_B$ )<sup>2</sup>/ $R_{ON}$ , where  $V_B$  is the reverse breakdown voltage and  $R_{ON}$  is the on-state resistance.<sup>1,3,4</sup> To achieve a high-power figure of merit, a rectifier must have a low drift layer concentration, with high electron mobility, as well as low  $R_{ON}$ , and optimized edge termination to prevent current crowding.<sup>1,5–21</sup> The breakdown voltage is larger for thicker drift layers, but this degrades the on-resistance. In addition, vertical geometry devices are desirable, because of their higher power conversion efficiency and absolute currents compared to lateral devices.<sup>1,3–5</sup> Power rectifiers are also building blocks for many advanced power handling systems.

The lack of a practical p-type doping capability for Ga<sub>2</sub>O<sub>3</sub> has led to integration with p-type oxides to form p-n heterojunctions with the n-type Ga<sub>2</sub>O<sub>3</sub>.<sup>9–16</sup> The most successful of these has been NiO, generally deposited by sputtering. The forward current transport mechanism in such junctions is typically recombination at low biases and trap-assisted tunneling at higher bias.<sup>10,21–26</sup> Promising rectifier performance has been reported with this approach,<sup>14–36</sup> including  $V_B$  of 8.32 kV, with figure of merit 13.2 GW cm<sup>-2</sup>.<sup>15</sup>

A less studied aspect has been the elevated temperature performance of such devices.<sup>37–42</sup> In this paper we report an

<sup>a</sup> Department of Chemical Engineering, University of Florida, Gainesville, FL 32606, USA

<sup>b</sup> Department of Materials Science and Engineering, University of Florida, Gainesville, FL 32606, USA. E-mail: spear@mse.ufl.edu

investigation of the temperature dependence of the performance of NiO/Ga<sub>2</sub>O<sub>3</sub> and also co-fabricated Au/Ni/Ga<sub>2</sub>O<sub>3</sub> vertical rectifiers on the same wafers. While the breakdown voltage of the latter fall-off quickly with increasing temperature, the heterojunction rectifiers exhibit nearly temperature-independent  $V_B$  to 600 K. While we focused on small area devices (100  $\mu$ m), we also fabricated a large area device (1 mm<sup>2</sup>) to examine the scaling properties.

## Experimental

We made both vertical geometry Schottky rectifiers and NiO/Ga<sub>2</sub>O<sub>3</sub> rectifiers on the same wafers. The bilayer NiO thickness of 10/10 nm and the length of the NiO extension beyond the top contact (12  $\mu$ m) to form the field plate-like overhang were held constant.<sup>17</sup> The drift region thickness was 10  $\mu$ m and these layers were grown by halide vapor phase epitaxy (HVPE) on a (001) Sn-doped (10<sup>19</sup> cm<sup>-3</sup>)  $\beta$ -Ga<sub>2</sub>O<sub>3</sub> single crystal substrate. The samples were purchased from Novel Crystal Technology, Japan. A schematic of the two device structures is shown in Fig. 1 (top).

Ohmic contacts were made to the back of the doped substrates using a Ti/Au deposited by e-beam evaporation and annealed at 550 °C for 180 s under N<sub>2</sub>. The front surface was cleaned by UV/Ozone exposure for 15 mins to remove contamination.<sup>17</sup> The 10/10 nm NiO bilayer was deposited after the Ohmic contacts by rf (13.56 MHz) magnetron sputtering at a working pressure of 3 mTorr. The hole concentration in these films was adjusted using the Ar/O<sub>2</sub> ratio. The structure was then annealed at 300 °C under O<sub>2</sub>. Finally, a top contact of 20/80 nm Ni/Au (100  $\mu$ m or 1 mm diameter) was deposited onto the NiO layer and also formed the Schottky contact on those devices. The NiO was extended 12  $\mu$ m beyond the contact metal to form a field-plate-like overhang.  $C^{-2}$ - $V$  plots for the drift layer doping showed that the carrier

concentration was  $6.7 \times 10^{15}$  cm<sup>-3</sup>. The device design for NiO thickness and extension was guided by TCAD simulations.<sup>17</sup>

The current density–voltage ( $J$ - $V$ ) characteristics were measured on Tektronix 370-A and 371-B curve tracers and an Agilent 4156C parameter analyser. For the reverse voltages >2 kV, a Glassman power supply was employed and all the measurements were performed in a Fluorinert atmosphere to avoid breakdown of the air at these high voltages. The reverse breakdown voltage was defined as the bias for a reverse current reaching 0.1 A cm<sup>-2</sup>. The devices did not suffer permanent damage under these conditions, with identical  $I$ - $V$  characteristics as before measurement, but increasing the voltage a further 50–200 V led to permanent failure through breakdown at the NiO/Ga<sub>2</sub>O<sub>3</sub> contact periphery. The on-resistance values were calculated assuming that the current spreading length is 10  $\mu$ m and a 45° spreading angle. We also subtracted the resistance of the cable, probe and chuck, which was around 10 Ohm.

## Results and discussion

Fig. 2 shows the forward  $J$ - $V$  characteristics and associated on-state resistances from (top) Schottky (SBD) rectifiers and (bottom) heterojunction (HJD) rectifiers of 100  $\mu$ m diameter as a function of temperature. The on-resistance was obtained from the slope of the forward  $I$ - $V$  characteristics. The turn-on voltages decrease with increasing temperature in both types of

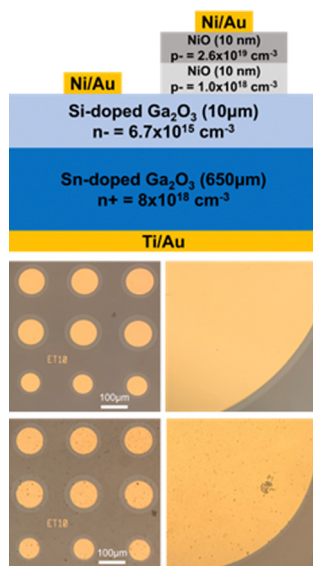


Fig. 1 (top) Schematic of the structures and images of devices (center) before and (bottom) after operation at 600 K.

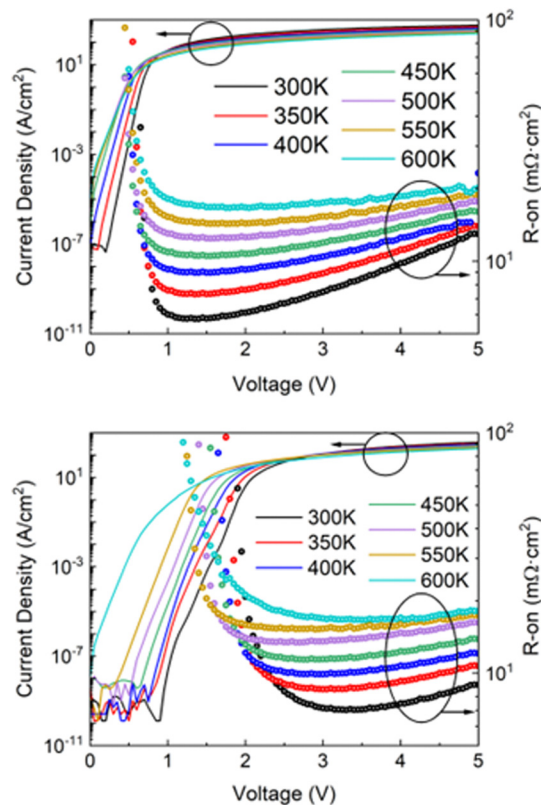


Fig. 2 Forward current densities and  $R_{ON}$  values for (top) Schottky rectifiers or (bottom) NiO/Ga<sub>2</sub>O<sub>3</sub> as a function of temperature.

devices, while  $R_{ON}$  increases due to the decreased carrier mobility at higher temperatures.<sup>4–6</sup> A Richardson plot for the Schottky rectifiers showed a  $e\Phi_{b0}$  value of 0.6 eV and a Richardson's constant of  $40 \text{ A cm}^{-2} \text{ K}^{-1}$ . The barrier height monotonically decreased from 1.02 eV at 300 K to 0.65 eV at 600 K. The  $R_{ON}$  values are slightly higher for the HJD, as expected.<sup>14–17</sup> Both types can conduct  $>100 \text{ A cm}^{-2}$  at 4 V. Note that the  $R_{ON}$  in the heterojunction rectifiers does not continue to decrease at forward voltages beyond  $\sim 3 \text{ V}$ . It has also been shown that the band alignment remains type II, staggered gap with the magnitude of the conduction and valence band offsets increasing monotonically with annealing temperature.<sup>12</sup>

Fig. 3 shows the reverse  $J$ - $V$  characteristics for both types of devices at different temperatures. The Schottky rectifiers show a sharp reduction in the breakdown voltage as temperature increases, as shown in Fig. 3 (top). By sharp contrast, the heterojunction rectifiers show very little change in breakdown voltage, as shown in Fig. 3 (bottom). Note also that the Schottky devices have breakdown voltages of only  $\sim 1100 \text{ V}$  at 300 K, whereas the NiO/Ga<sub>2</sub>O<sub>3</sub> devices remain above 8 kV across the temperature range up to 600 K. This is a remarkable demonstration of the utility of NiO in forming a robust p-n junction with Ga<sub>2</sub>O<sub>3</sub> and also in providing effective edge termination to mitigate breakdown at the contact periphery. The devices did not show any visible damage after measurement at 600 K, as shown in the center and bottom of Fig. 1 for the Schottky and heterojunction rectifiers, respectively.

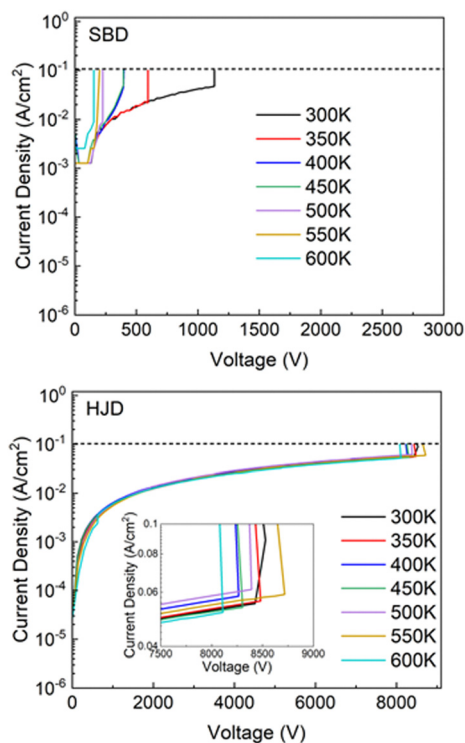


Fig. 3 (top) Reverse current characteristics from Schottky rectifiers and (bottom) NiO/Ga<sub>2</sub>O<sub>3</sub> heterojunction rectifiers as a function of temperature.

To give an example of the uniformity of the results, Fig. 4 (top) shows the spread of the reverse current characteristics from eight different NiO/Ga<sub>2</sub>O<sub>3</sub> heterojunction rectifiers at 300 K. This was from 7.9–8.7 kV, measured over an area of approximately  $1 \text{ cm}^2$ . The trends in  $V_B$  with temperature are shown in Fig. 4 (bottom) for the two device types, with the same number of Schottky diodes measured. While the heterojunction devices show no significant change in  $V_B$  up to 600 K, the Schottky rectifiers show the commonly reported negative temperature coefficient. The temperature dependence of  $V_B$  follows an approximate relationship of the form:<sup>4,37–42</sup>

$$V_B = V_{B0}[1 + \beta(T - T_0)]$$

where  $\beta = -2 \pm 0.6 \text{ V K}^{-1}$ . The negative temperature coefficient precludes impact ionization as the breakdown mechanism in the Schottky rectifiers. This is not unexpected, as new materials technologies generally show breakdowns dominated by defect-assisted processes until the material growth matures. This was the case for GaN, for example.<sup>43</sup> Previous work has shown in vertical geometry Ga<sub>2</sub>O<sub>3</sub> rectifiers that impact ionization of deep acceptors is a strong contributor to breakdown.<sup>44</sup> A low or negative temperature coefficient of breakdown does have advantages in preventing the rectifiers from being damaged by excessive voltage. A positive temperature coefficient of breakdown can lead to overvoltage conditions and device failure at high temperatures.

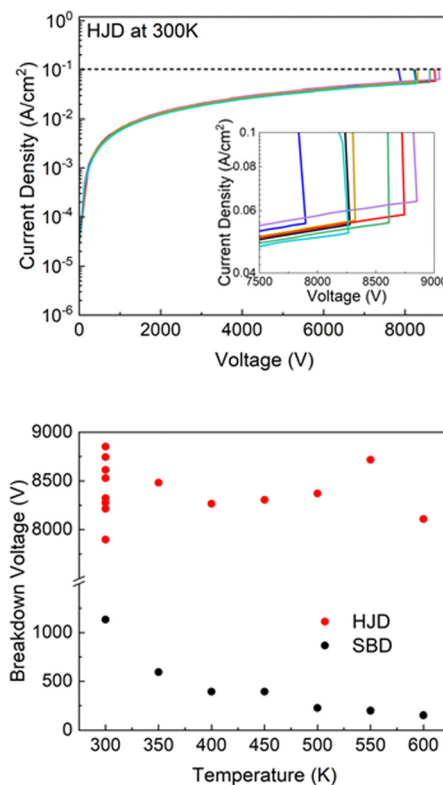


Fig. 4 (top) Spread of reverse current characteristics from NiO/Ga<sub>2</sub>O<sub>3</sub> heterojunction rectifiers at 300 K. (bottom) Temperature dependence of breakdown voltage for Schottky barrier diodes and heterojunction diodes.

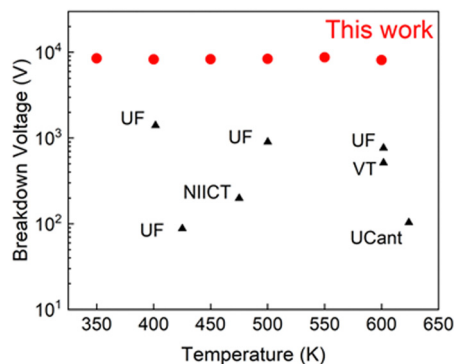


Fig. 5 Compilation of maximum operation temperature *versus*  $V_B$  for vertical  $\text{Ga}_2\text{O}_3$  rectifiers. Previous data comes from Virginia Tech<sup>37</sup>, University of Canterbury<sup>39</sup>, University of Florida<sup>38</sup> and NIICT<sup>40</sup>.

Fig. 5 shows a compilation of reported maximum operation temperature *versus*  $V_B$  for vertical  $\text{Ga}_2\text{O}_3$  rectifiers. There is a clear improvement in the present work, which we ascribe to the advances in crystal growth in lowering the drift layer carrier concentration and extended defect density in the starting wafers and also to optimization of the NiO deposition parameters.

The  $R_{\text{ON}}$  and turn-on voltages from the Schottky and heterojunction rectifiers are shown as a function of temperature in Fig. 6. The  $R_{\text{ON}}$  values are higher for the heterojunctions and increase with temperature, which we ascribe mainly to the degradation in carrier mobility through phonon (lattice)

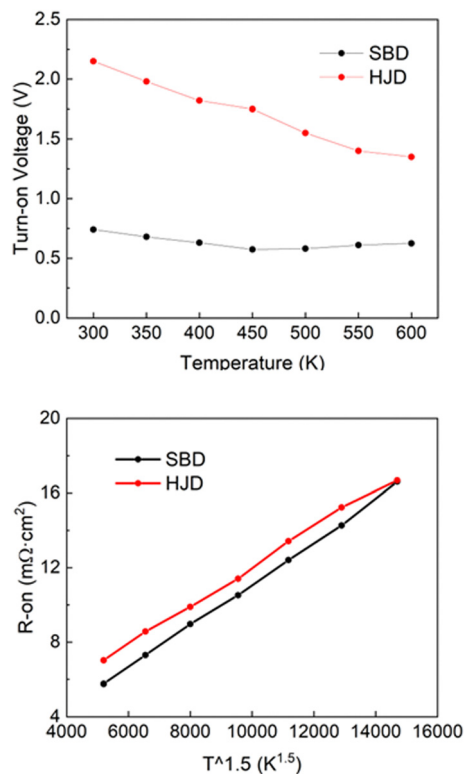


Fig. 6 Temperature dependence of on-state resistance and turn-on voltage for Schottky barrier diodes and heterojunction diodes.

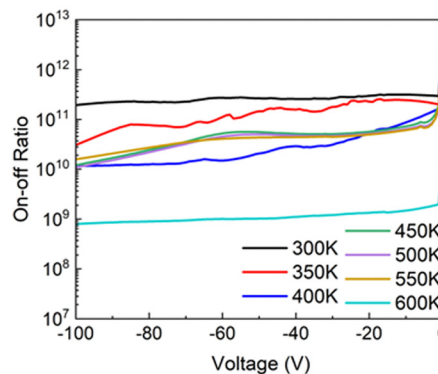
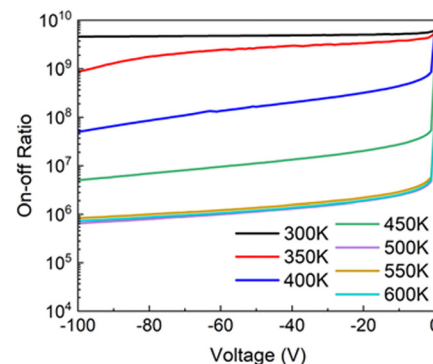


Fig. 7 On-off ratio of (top) Schottky rectifiers and (bottom) NiO/ $\text{Ga}_2\text{O}_3$  heterojunction rectifiers in which the bias was switched from 5 V forward to the voltage shown on the x-axis.

scattering since we could fit the  $R_{\text{ON}}$  data to a  $T^{3/2}$  dependence. Additional evidence could come from extracting mobility from the space charge limited current *via* the Mott–Gurney Law. The turn-on voltage exhibited a weak dependence on temperature and was lower for the Schottky rectifiers, as expected. The power figure of merits for the heterojunctions were  $9.1 \text{ GW cm}^{-2}$  at 300 K and  $3.9 \text{ GW cm}^{-2}$  at 600 K. Note that the theoretical maximum is around  $34 \text{ MW cm}^{-2}$ . The corresponding figures of merit for Schottky rectifiers were  $0.22 \text{ GW cm}^{-2}$  at 300 K and  $0.59 \text{ MW cm}^{-2}$  at 600 K.

The on-off ratios as a function of temperature when switching from 5 V forward bias to the negative voltages shown on the

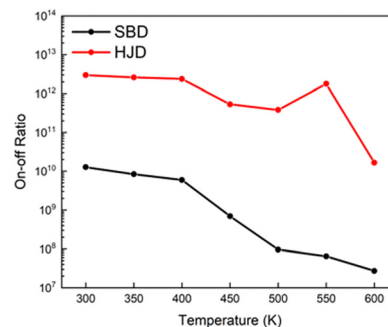


Fig. 8 Temperature dependence of the on/off ratio for Schottky barrier diodes and heterojunction diodes when switching from 5 V forward to 0 V.



x-axes are shown in Fig. 7 for both types of rectifiers. The values are 1–3 orders of magnitude higher for the heterojunctions due to the lower reverse current at a given bias. Even at 600 K the on–off ratio is  $\sim 10^9$  for the NiO/Ga<sub>2</sub>O<sub>3</sub> rectifiers.

Fig. 8 shows the temperature dependence of the on/off ratio for (top) Schottky barrier diodes and (bottom) heterojunction diodes for switching from 5 V forward voltage to 0 V. These are essentially the maximum on–off ratios achievable in the devices.

The switching characteristics of the rectifiers are also of paramount interest, since they need fast recovery times and the ability to switch large currents.<sup>45–63</sup> Fig. 9 shows the temperature dependence of (top) Schottky rectifiers and (bottom) NiO/Ga<sub>2</sub>O<sub>3</sub> heterojunction rectifiers of reverse recovery characteristics in which the devices were switched from 60 mA forward current to 0 V. The reverse recovery times are  $\sim 26 \pm 2$  ns and are tabulated in Table 1. The relative indifference to device structure and temperature demonstrates that charge storage in the p–n junction is not a significant factor compared to the Schottky device. We have not seen a significant difference in recovery characteristics between small and large devices.

We also examined the temperature dependence of the performance of the large area (1 mm<sup>2</sup>) heterojunction rectifiers. Fig. 10 (top) shows the forward current characteristics. Note that the absolute forward current is  $> 3$  A for all temperatures, with a breakdown voltage of 4 kV at room temperature, as shown in Fig. 10 (bottom). The reason for the lower breakdown is not clear and could be due to a higher probability of having intrinsic defects or an issue with field crowding. The power figure-of-merit is 6.4 GW cm<sup>-2</sup> at 300 K and 0.8 MW cm<sup>-2</sup> at

Table 1 Recovery characteristics from Schottky and heterojunction rectifiers

Temperature (K)	Trr (ns)	Irr (mA)	dI/dT (A μs <sup>-1</sup> )	IF (mA)
Schottky				
300	24	-23	2.7	60
350	28	-26	2.6	60
400	28	-27	2.5	60
450	25	-26	2.3	60
500	27	-25	2.1	60
550	26	-26	2.3	60
600	24	-26	2.2	60
Heterojunction				
300	25	-20	2.4	60
350	25	-27	2.0	60
400	25	-27	2.0	60
450	25	-27	1.9	60
500	23	-26	1.9	60
550	25	-24	1.9	60
600	27	-25	1.9	60

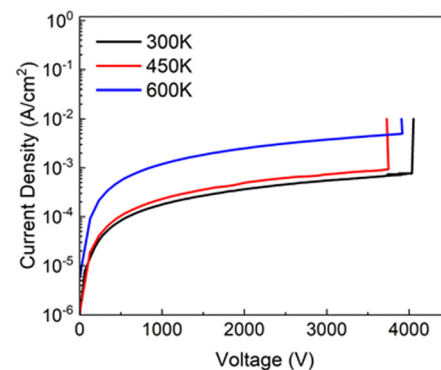
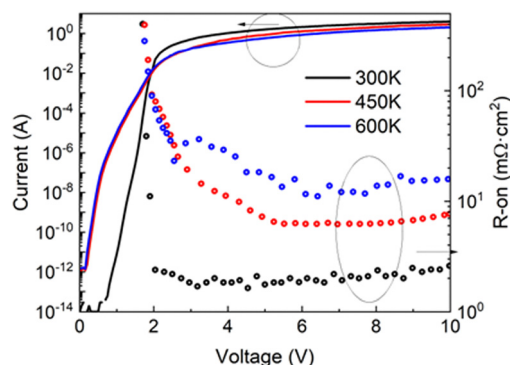


Fig. 10 (top) Forward current densities and  $R_{ON}$  values and (bottom) reverse current characteristics from 1 mm<sup>2</sup> NiO/Ga<sub>2</sub>O<sub>3</sub> heterojunction rectifiers as a function of temperature.

600 K. The on–off ratio remained above  $10^8$  at 600 K, for switching to  $-100$  V, as shown in Fig. 11.

## Conclusions

Since the breakdown, forward  $I$ – $V$  and on resistance did not degrade to much at 300 °C, the concerns of low thermal conductivity of gallium oxide should be of less concern

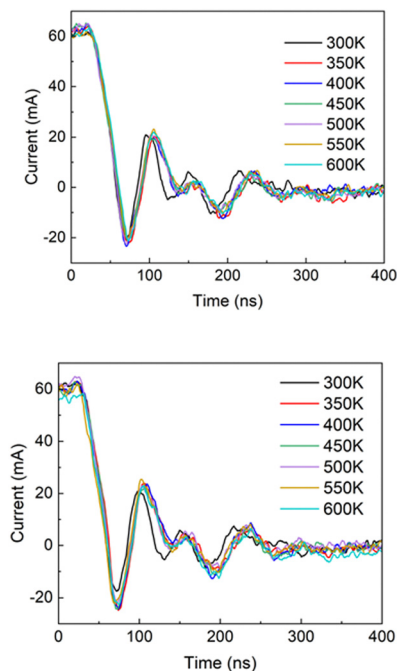


Fig. 9 Temperature dependence of switching characteristics of (top) Schottky rectifiers and (bottom) NiO/Ga<sub>2</sub>O<sub>3</sub> heterojunction rectifiers in which the devices were switched from 60 mA forward current to zero.

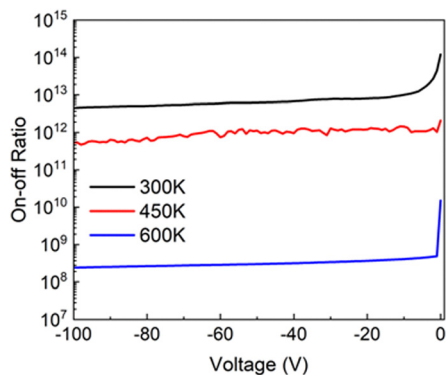


Fig. 11 On-off ratio of 1 mm<sup>2</sup> NiO/Ga<sub>2</sub>O<sub>3</sub> heterojunction rectifiers in which the bias was switched from 10 V forward to the voltage shown on the x-axis.

provided the long-term reliability can be established. The power figure of merits reported here are around 26% of the theoretical maximum for Ga<sub>2</sub>O<sub>3</sub>.<sup>15</sup> It is anticipated that continued reduction in defect density, as well as adding other edge termination technology such as field plates, implanted guard rings, and mesa etching as possible methods to improve field uniformity can enhance future performance closer to this maximum. This is because bulk Ga<sub>2</sub>O<sub>3</sub> crystals are known to have internal planar defects, *i.e.*, plate-like voids and stacking faults, and it is known that higher dislocation densities lead to higher leakage currents in Ga<sub>2</sub>O<sub>3</sub> rectifiers.<sup>64–66</sup> This is because the dislocations can act as recombination centers for electrons and holes, leading to an increased probability of carrier recombination and subsequent leakage current and hence lower breakdown voltage.

The NiO/Ga<sub>2</sub>O<sub>3</sub> heterojunction rectifier is potentially an ideal structure for high-voltage and high-power applications, where it can offer better efficiency and reduced energy losses compared to traditional semiconductors. The wide bandgap of both NiO (~3.9 eV) and β-Ga<sub>2</sub>O<sub>3</sub> (4.8 eV) also makes power rectifiers from this heterojunction attractive for high-temperature applications. These properties make Ga<sub>2</sub>O<sub>3</sub> power rectifiers promising for high-power and high-temperature applications such as electric vehicles, power electronics, and aerospace.

## Conflicts of interest

There are no conflicts to declare.

## Acknowledgements

The work at UF was performed as part of the Interaction of Ionizing Radiation with Matter University Research Alliance (IIRM-URA), sponsored by the Department of the Defense, Defense Threat Reduction Agency under award HDTRA1-20-2-0002. The content of the information does not necessarily reflect the position or the policy of the federal government, and no official endorsement should be inferred. The work at UF was also supported by NSF DMR 1856662.

## References

- M. H. Wong and M. Higashiwaki, *IEEE Trans. Electron Devices*, 2020, **67**, 3925.
- Z. Galazka, *J. Appl. Phys.*, 2022, **131**, 031103.
- X. Lu, Y. X. Deng, Y. L. Pei, Z. M. Chen and G. Wang, *J. Semicond.*, 2023, **44**, 061802.
- A. J. Green, J. Speck, G. Xing, P. Moens, F. Allerstam, K. Gumaelius, T. Neyer, A. Arias-Purdue, V. Mehrotra, A. Kuramata, K. Sasaki, S. Watanabe, K. Koshi, J. Blevins, O. Bierwagen, S. Krishnamoorthy, K. Leedy, A. R. Arehart, A. T. Neal, S. Mou, S. A. Ringel, A. Kumar, A. Sharma, K. Ghosh, U. Singiseti, W. Li, K. Chabak, K. Liddy, A. Islam, S. Rajan, S. Graham, S. Choi, Z. Cheng and M. Higashiwaki, *APL Mater.*, 2022, **10**, 029201.
- S. J. Pearton, F. Ren, M. Tadjer and J. Kim, *J. Appl. Phys.*, 2018, **124**, 220901.
- C. Wang, J. Zhang, S. Xu, C. Zhang, Q. Feng, Y. Zhang, J. Ning, S. Zhao, H. Zhou and Y. Hao, *J. Phys. D: Appl. Phys.*, 2021, **54**, 243001.
- M. Bosi, P. Mazzolini, L. Seravalli and R. Fornari, *J. Mater. Chem. C*, 2020, **8**, 10975.
- K. Kaneko, K. Uno, R. Jinno and S. Fujit, *J. Appl. Phys.*, 2022, **131**, 090902.
- Y. Kokubun, S. Kubo and S. Nakagomi, *Appl. Phys. Express*, 2016, **9**, 091101.
- Y. Deng, Z. Yang, T. Xu, H. Jiang, K. W. Ng, C. Liao, D. Su, Y. Pei, Z. Chen, G. Wang and X. Lu, *Appl. Surf. Sci.*, 2023, **622**, 156917.
- M. I. Pintor-Monroy, D. Barrera, B. L. Murillo-Borjas, F. Javier Ochoa-Estrella, J. W. P. Hsu and M. A. Quevedo-Lopez, *ACS Appl. Mater. Interfaces*, 2018, **10**, 38159.
- X. Xia, J.-S. Li, C.-C. Chiang, T. J. Yoo, F. Ren, H. Kim and S. J. Pearton, *J. Phys. D: Appl. Phys.*, 2022, **55**, 385105.
- H. Gong, X. Chen, Y. Xu, Y. Chen, F. Ren, B. Liu, S. Gu, R. Zhang and J. Ye, *IEEE Trans. Electron Devices*, 2020, **67**, 3341.
- S. Sharma, K. Zeng, S. Saha and U. Singiseti, *IEEE Trans. Electron Devices*, 2020, **41**, 836.
- J. Zhang, P. Dong, K. Dang, Y. Zhang, Q. Yan, H. Xiang, J. Su, Z. Liu, M. Si, J. Gao, M. Kong, H. Zhou and Y. Hao, *Nat. Commun.*, 2022, **13**, 3900.
- P. Dong, J. Zhang, Q. Yan, Z. Liu, P. Ma, H. Zhou and Y. Hao, *IEEE Trans. Electron Devices*, 2022, **43**, 765.
- J.-S. Li, C.-C. Chiang, X. Xia, T. Jinsoo Yoo, F. Ren, H. Kim and S. J. Pearton, *Appl. Phys. Lett.*, 2022, **121**, 042105.
- Y. Lv, Y. Wang, X. Fu, S. Dun, Z. Sun, H. Liu, X. Zhou, X. Song, K. Dang, S. Liang, J. Zhang, H. Zhou, Z. Feng, S. Cai and Y. Hao, *IEEE Trans. Power Electr.*, 2021, **36**, 6179.
- C. Liao, X. Lu, T. Xu, P. Fang, Y. Deng, H. Luo, Z. Wu, Z. Chen, J. Liang, Y. Pei and G. Wang, *IEEE Trans. Electron Devices*, 2022, **69**, 5722.
- M. Xiao, B. Wang, J. Liu, R. Zhang, Z. Zhang, C. Ding, S. Lu, K. Sasaki, G.-Q. Lu, C. Buttay and Y. Zhang, *IEEE Trans. Power Electr.*, 2021, **36**, 8565.

- 21 X. Lu, X. Zhou, H. Jiang, K. Wei Ng, Z. Chen, Y. Pei, K. May Lau and G. Wang, *IEEE Electron Device Lett.*, 2020, **41**, 449.
- 22 C. Wang, H. Gong, W. Lei, Y. Cai, Z. Hu, S. Xu, Z. Liu, Q. Feng, H. Zhou, J. Ye, J. Zhang, R. Zhang and Y. Hao, *IEEE Electron Device Lett.*, 2021, **42**, 485.
- 23 Q. Yan, H. Gong, J. Zhang, J. Ye, H. Zhou, Z. Liu, S. Xu, C. Wang, Z. Hu, Q. Feng, J. Ning, C. Zhang, P. Ma, R. Zhang and Y. Hao, *Appl. Phys. Lett.*, 2021, **118**, 122102.
- 24 H. H. Gong, X. H. Chen, Y. Xu, F.-F. Ren, S. L. Gu and J. D. Ye, *Appl. Phys. Lett.*, 2020, **117**, 022104.
- 25 H. Gong, F. Zhou, W. Xu, X. Yu, Y. Xu, Y. Yang, F.-F. Ren, S. Gu, Y. Zheng, R. Zhang, H. Lu and J. Ye, *IEEE Trans. Power Electr.*, 2021, **36**, 12213.
- 26 H. H. Gong, X. X. Yu, Y. Xu, X. H. Chen, Y. Kuang, Y. J. Lv, Y. Yang, F.-F. Ren, Z. H. Feng, S. L. Gu, Y. D. Zheng, R. Zhang and J. D. Yue, *Appl. Phys. Lett.*, 2021, **118**, 202102.
- 27 W. Hao, Q. He, K. Zhou, G. Xu, W. Xiong, X. Zhou, G. Jian, C. Chen, X. Zhao and S. Long, *Appl. Phys. Lett.*, 2021, **118**, 043501.
- 28 F. Zhou, H. Gong, W. Xu, X. Yu, Y. Xu, Y. Yang, F.-F. Ren, S. Gu, Y. Zheng, R. Zhang, J. Ye and H. Lu, *IEEE Trans. Power Electr.*, 2022, **37**, 1223.
- 29 Q. Yan, H. Gong, H. Zhou, J. Zhang, J. Ye, Z. Liu, C. Wang, X. Zheng, R. Zhang and Y. Hao, *Appl. Phys. Lett.*, 2022, **120**, 092106.
- 30 Y. J. Lv, Y. G. Wang, X. C. Fu, S. B. Dun, Z. F. Sun, H. Y. Liu, X. Y. Zhou, X. B. Song, K. Dang, S. X. Liang, J. C. Zhang, H. Zhou, Z. H. Feng, S. J. Cai and Y. Hao, *IEEE Trans. Power Electr.*, 2021, **36**, 6179.
- 31 J. Zhang, S. Han, M. Cui, X. Xu, W. Li, H. Xu, C. Jin, M. Gu, L. Chen and K. H. L. Zhang, *ACS Appl. Electron. Mater.*, 2020, **2**, 456.
- 32 Y. Wang, H. Gong, Y. Lv, X. Fu, S. Dun, T. Han, H. Liu, X. Zhou, S. Liang, J. Ye, R. Zhang, A. Bu, S. Cai and Z. Feng, *IEEE Trans. Power Electr.*, 2022, **37**, 3743.
- 33 J.-S. Li, C.-C. Chiang, X. Xia, H.-H. Wan, F. Ren and S. J. Pearton, *J. Vac. Sci. Technol. A*, 2023, **41**, 030401.
- 34 Z. Wang, H. Gong, S. Member, C. Meng, X. Yu, X. Sun, C. Zhang, X. Ji, F. Ren, S. Gu, Y. Zheng, R. Zhang and J. Ye, *IEEE Trans. Electron Devices*, 2022, **69**, 981.
- 35 B. Wang, M. Xiao, J. Spencer, Y. Qin, K. Sasaki, M. J. Tadjer and Y. Zhang, *IEEE Electron Device Lett.*, 2023, **44**, 221.
- 36 F. Zhou, H. H. Gong, Z. P. Wang, W. Z. Xu, X. X. Yu, Y. Yang, F.-F. Ren, S. L. Gu, R. Zhang, Y. D. Zheng, H. Lu and J. D. Ye, *Appl. Phys. Lett.*, 2021, **119**, 262103.
- 37 B. Wang, M. Xiao, X. Yan, H. Y. Wong, J. Ma, K. Sasaki, H. Wang and Y. Zhang, *Appl. Phys. Lett.*, 2019, **115**, 263503.
- 38 X. Xia, M. Xian, P. Carey, C. Fares, F. Ren, M. Tadjer, S. J. Pearton, T. Quang Tu, K. Goto and A. Kuramata, *J. Phys. D: Appl. Phys.*, 2021, **54**, 305103.
- 39 C. Hou, K. R. York, R. A. Makin, S. M. Durbin, R. M. Gazoni, R. J. Reeves and M. W. Allen, *Appl. Phys. Lett.*, 2020, **117**, 203502.
- 40 S. Ahn, F. Ren, L. Yuan, S. J. Pearton and A. Kuramata, *ECS J. Solid State Sci. Technol.*, 2017, **6**, P68.
- 41 M. Higashiwaki, K. Konishi, K. Sasaki, K. Goto, K. Nomura, Q. T. Thieu and R. Togashi, *Appl. Phys. Lett.*, 2016, **108**, 133503.
- 42 W. Hao, Q. He, X. Zhou, X. Zhao, G. Xu and S. Long, 2.6 kV NiO/Ga<sub>2</sub>O<sub>3</sub> Heterojunction Diode with Superior High-Temperature Voltage Blocking Capability, 2022 IEEE 34th International Symposium on Power Semiconductor Devices and ICs (ISPSD), Vancouver, BC, Canada, 2022, pp. 105–108.
- 43 L. Cao, Z. Zhu, G. Harden, H. Ye, J. Wang, A. Hoffman and P. Fay, *IEEE Trans. Electron Devices*, 2021, **68**, 1228.
- 44 E. B. Yakimov, A. Y. Polyakov, I. V. Shchemerov, N. B. Smirnov, A. A. Vasilev, A. I. Kochkova, P. S. Vergeles, E. E. Yakimov, A. V. Chernykh, M. Xian, F. Ren and S. J. Pearton, *J. Alloys Compd.*, 2021, **879**, 160394.
- 45 W. Hao, F. Wu, W. Li, G. Xu, X. Xie, K. Zhou, W. Guo, X. Zhou, Q. He, X. Zhao, S. Yang and S. Long, High-Performance Vertical  $\beta$ -Ga<sub>2</sub>O<sub>3</sub> Schottky Barrier Diodes Featuring P-NiO JTE with Adjustable Conductivity, 2022 International Electron Devices Meeting (IEDM), San Francisco, CA, USA, 2022, pp. 9.5.1–9.5.4.
- 46 X. Zhou, Q. Liu, W. Hao, G. Xu and S. Long, Normally-off  $\beta$ -Ga<sub>2</sub>O<sub>3</sub> Power Heterojunction Field-Effect-Transistor Realized by p-NiO and Recessed-Gate, 2022 IEEE 34th International Symposium on Power Semiconductor Devices and ICs (ISPSD), Vancouver, BC, Canada, 2022, pp. 101–104.
- 47 Y. Qin, Z. Wang, K. Sasaki, J. Ye and Y. Zhang, *Jpn J. Appl. Phys.*, 2023, **62**, SF0801.
- 48 H. Gong, F. Zhou, W. Xu, X. Yu, Y. Xu, Y. Yang, F. Ren, S. Gu, Y. Zheng and R. Zhang, *IEEE Trans. Power Electr.*, 2021, **36**, 12213.
- 49 J. Yang, C. Fares, R. Elhassani, M. Xian, F. Ren, S. J. Pearton, M. Tadjer and A. Kuramata, *ECS J. Solid State Sci. Technol.*, 2019, **8**, Q3159.
- 50 M. Ji, N. R. Taylor, I. Kravchenko, P. Joshi, T. Aytug, L. R. Cao and M. P. Paranthaman, *IEEE Trans. Power Electr.*, 2020, **36**, 41.
- 51 Z. Islam, M. Xian, A. Haque, F. Ren, M. Tadjer and S. J. Pearton, *IEEE Trans. Electron Devices*, 2020, **67**, 3056.
- 52 R. Sun, A. R. Balog, H. Yang, N. Alem and M. A. Scarpulla, *IEEE Electron Device Lett.*, 2023, **44**(5), 725–728.
- 53 M. Xiao, B. Wang, J. Liu, R. Zhang, R. Zhang, C. Ding, S. Lu, K. Sasaki, G. Q. Lu, C. Buttay and Y. Zhang, *IEEE Trans. Power Electr.*, 2021, **36**, 8565.
- 54 H. Gong, F. Zhou, X. Yu, W. Xu, F. Ren, S. Gu, H. Lu, J. Ye and R. Zhang, *IEEE Electron Device Lett.*, 2022, **43**, 773.
- 55 F. Otsuka, H. Miyamoto, A. Takatsuka, S. Kunori, K. Sasaki and A. Kuramata, *Appl. Phys. Express*, 2021, **15**, 016501.
- 56 W. Hao, F. Wu, W. Li, G. Xu, X. Xie, K. Zhou, W. Guo, X. Zhou, Q. He, X. Zhao and S. Yang, 2022, December. High-Performance Vertical  $\beta$ -Ga<sub>2</sub>O<sub>3</sub> Schottky Barrier Diodes Featuring P-NiO JTE with Adjustable Conductivity. In 2022 International Electron Devices Meeting (IEDM) (pp. 9–5). IEEE.
- 57 Y. Lv, Y. Wang, X. Fu, S. Dun, Z. Sun, H. Liu, X. Zhou, X. Song, K. Dang, S. Liang and J. Zhang, *IEEE Trans. Power Electr.*, 2020, **3**, 6179.
- 58 J. Wei, Y. Wei, J. Lu, X. Peng, Z. Jiang, K. Yang and X. Luo, 2022, May. Experimental Study on Electrical Characteristics of Large-Size Vertical  $\beta$ -Ga<sub>2</sub>O<sub>3</sub> Junction Barrier Schottky

- Diodes. In 2022 IEEE 34th International Symposium on Power Semiconductor Devices and ICs (ISPSD) (pp. 97–100). IEEE.
- 59 J. Yang, F. Ren, Y.-T. Chen, Y.-T. Liao, C.-W. Chang, J. Lin, M. J. Tadjer, S. J. Pearton and A. Kuramata, *IEEE J. Electron Devices Soc.*, 2019, 7, 57.
- 60 J.-S. Li, C.-C. Chiang, X. Xia, F. Ren and S. J. Pearton, *J. Vac. Sci. Technol., A*, 2022, 40, 063407.
- 61 F. Zhou, H. H. Gong, Z. P. Wang, W. Z. Xu, X. X. Yu, Y. Yang, F. F. Ren, S. L. Gu, R. Zhang, Y. D. Zheng and H. Lu, *Appl. Phys. Lett.*, 2021, 119, 262103.
- 62 F. Zhou, H. Gong, W. Xu, X. Yu, Y. Xu, Y. Yang, F. F. Ren, S. Gu, Y. Zheng, R. Zhang and J. Ye, *IEEE Trans. Power Electr.*, 2021, 37, 1223.
- 63 J. S. Li, C. C. Chiang, X. Xia, C. T. Tsai, F. Ren, Y. T. Liao and S. J. Pearton, *ECS J. Solid State Sci. Technol.*, 2022, 11, 105003.
- 64 S. Sdoeung, K. Sasaki, K. Kawasaki, J. Hirabayashi, A. Kuramata and M. Kasu, *Jpn. J. Appl. Phys.*, 2023, 62, SF1001.
- 65 B. Wang, M. Xiao, J. Knoll, C. Buttay, K. Sasaki, C. Dimarino and Y. Zhang, *IEEE Electron Device Lett.*, 2021, 42, 1132.
- 66 K. Ogawa, N. Ogawa, R. Kosaka, T. Isshiki, Y. Yao and Y. Ishikawa, *J. Electron. Mater.*, 2020, 49, 5190.